OncoTargets and Therapy

Dovepress
open access to scientific and medical research

Open Access Full Text Article

ORIGINAL RESEARCH

B7 Induces Apoptosis in Colorectal Cancer Cells by Regulating the Expression of Caspase-3 and Inhibits Autophagy

Xinyi Zhang[1], Fengxi Li[2], Rong Li[1], Nan Zhao[2], Dianfeng Liu[1], Yuelin Xu[2], Lei Wang[2], Dongxu Wang[1], Ruihong Zhao[3]

[1]Laboratory Animal Center, College of Animal Science, Jilin University, Changchun, 130062, People's Republic of China; [2]Key Laboratory of Molecular Enzymology and Engineering of Ministry of Education, School of Life Sciences, Jilin University, Changchun, 130023, People's Republic of China; [3]Department of Gastroenterology Endoscopy Center, The First Hospital of Jilin University, Changchun, 130021, People's Republic of China

Correspondence: Dongxu Wang, Laboratory Animal Center, College of Animal Science, Jilin University, Changchun, 130062, People's Republic of China, Tel +86-18743089730; +86-0431-87836570, Email wang_dong_xu@jlu.edu.cn; Ruihong Zhao, Department of Gastroenterology Endoscopy Center, The First Hospital of Jilin University, Changchun, 130062, People's Republic of China, Tel +86-18844115258; +86-0431-87836578, Email ruihongzhao8@jlu.edu.cn

Purpose: Heterocyclic compounds are organic compounds with heterocyclic structures, which are common in drug molecules. They include pyrazines with diverse functions, including anti-cancer, antimicrobial, antidiabetic, and anticholinergic activities. In this study a new small molecular compound B7 based on tetrazolium substituted pyrazine was synthesized and its effect on the progression of colorectal cancer (CRC) and its potential mechanism were investigated.

Methods: We synthesized a series of tetrazolium-substituted pyrazine compounds by chemoenzymatic method. NCM460 (Human), HCT116 (Human), SW480 (Human) cell lines were selected to analyse the inhibitory effect of B7 on CRC by CCK-8, apoptosis, cell migration and invasion, qPCR, Western blotting, molecular docking, immunofluorescence. Moreover, a CRC xenograft model of mice was used to analyzed the role of B7 in vivo.

Results: Among these compounds, 3-methyl-5je-6-bis (1H-tetrazole-5-yl) pyrazine-2-carboxylic acid (B7) inhibited CRC cell proliferation and induced apoptosis. The expression of Caspase-3 was increased after B7 treatment. In addition, the mitochondria abnormalities was observed in B7 group due to decrease the expression of Beclin-1. In addition, B7 inhibited the migration and invasion in CRC cells. Finally, the results showed that B7 had anti-tumor activity in CRC xenograft model of mice.

Conclusion: In summary, compound B7 was synthesized efficiently using tetrazolium-substituted pyrazine via a chemoenzymatic method. Moreover, B7 have ability to regulate the expression of Caspase-3 which induced apoptosis in CRC cells. In addition, decreased Beclin-1 expression after B7 treatment, indicating inhibited autophagy. This study showed that B7 effectively induced apoptosis and inhibited autophagy in CRC cells.

Keywords: pyrazines, tetrazoles, colorectal cancer, apoptosis, autophagy

Introduction

Colorectal cancer (CRC) is the tumor which is a leading cause of cancer death worldwide.[1] The primary causation of death with CRC may be the high invasion and metastasis of CRC cells.[2] CRC treatments have progressed, the patients' five-year survival rate with advanced CRC remains inferior.[3] Resection and chemotherapy are currently two main CRC treatments.[4] Chemotherapy can relieve symptoms and lengthen the span of patients' life with advanced CRC. However, it does not have significant improvement of clinical outcome of patients with recurrent or metastatic drug-resistant CRC.[5,6] While many chemotherapeutic drugs, such as 5-fluorouracil and hydroxyurea, have high efficiency, their non-specific organ distribution in the body causes diverse clinical side effects.[7] Therefore, developing innovative drugs to suppress the growth of CRC cells with lower toxicity is essential.

Received: 28 July 2023
Accepted: 18 October 2023
Published: 27 October 2023

Pyrazine derivatives are heterocyclic compounds with various biological activities, including anticancer, antimicrobial, antidiabetic, and anticholinergic.[8–13] Tetrazole derivatives, an important synthetic heterocycle scaffold, are widely used in medicine, biochemistry, and pharmacology.[14–20] Tetrazole rings exist in many drugs due to bioisomerism, metabolic stability, and other physicochemical properties beneficial to carboxylic acids and amide moieties.[21,22] Therefore, tetrazole containing pyrazine combines tetrazole and pyrazine moieties, which may provide strategies for new drug development (Figure 1). Despite continuing problems, heterocycle synthesis has significantly progressed. Nowadays, multidisciplinary tools and strategies have increasingly been used to address this issue. Biocatalysis offers an alternative approach to conventional chemical processes with high selectivity and mild reaction conditions.[23,24] Organic chemists are currently looking for a combination of biocatalysis and synthetic organic methods to rapidly effectively construct complex molecules.[25–27]

In this study, we aimed to the synthesis of tetrazole-substituted pyrazine compounds B7 by chemoenzymatic method. The effects of B7 on the proliferation, migration, invasion, apoptosis and autophagy were analyzed in CRC cells. In order to verify the effect of B7 on apoptosis and autophagy, we analyzed the expression of apoptosis-related genes, such as Caspase-3, and autophagy-related genes, such as *Beclin-1*. In addition, the effect of B7 on tumor growth in vivo were evaluated.

Materials and Methods

Chemical Materials

Hemoglobin from bovine blood (HbBv) was obtained from Shanghai YuanYe Bio-Tec Company (Shanghai, China). Diaminomaleonitrile was bought from J&K Scientific (Beijing, China). α-Diazo-β-carbonyl compounds were synthesized using a reported method 25. All chemical reagents were bought from Shanghai Chemical Reagent Company (Shanghai, China).

General Procedure for Synthesizing Nitrile-Substituted Pyrazine (3)

A mixture of diaminomaleonitrile (1, 1.0 mmol) was obtained by mixing α-diazo-β-carbonyl compounds (2, 1.0 Equiv), HbBv (0.1 mol%), water (2 mL) and Triton X-100 (5% mol) and stirring the solution in a pre-heated constant temperature shaker (THZ-98A; Shanghai Yiheng, China) at 55°C until the reaction completed, as shown by thin-layer chromatography. Next the mixture was inburst into 10 mL of water, drawn with ethyl acetate (2× 10 mL). Then, synthetic organic layer was cleaned using an aqueous ammonium chloride solution and air-dried over magnesium sulfate ($MgSO_4$).

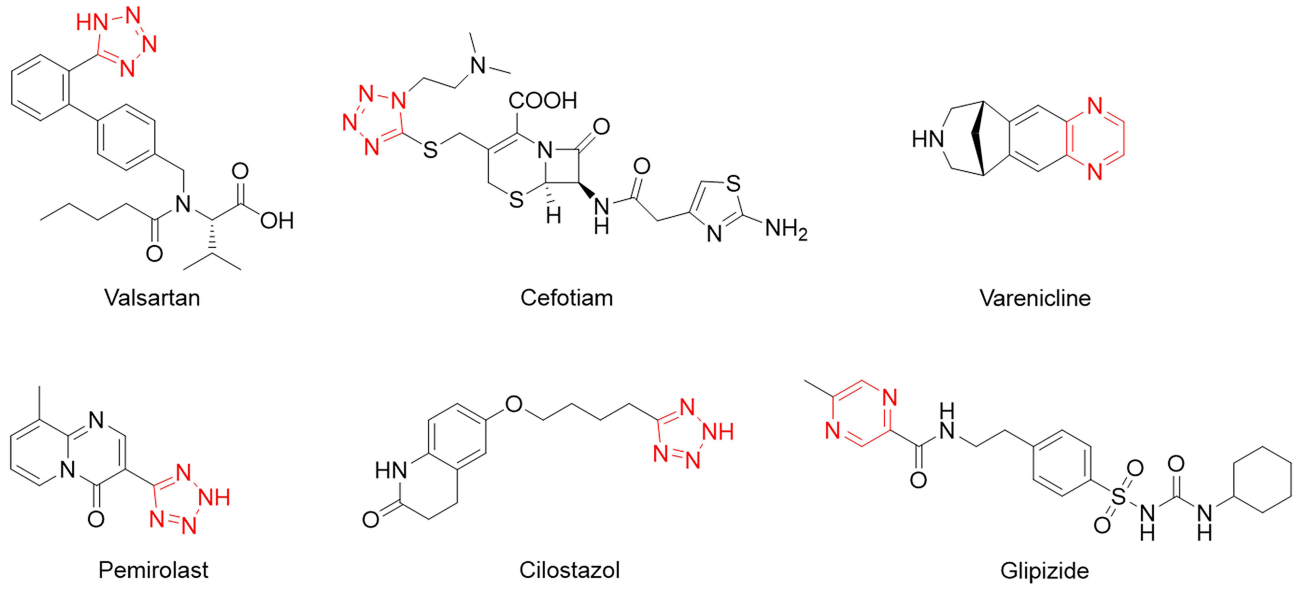

Figure 1 A bioactive pyrazine and tetrazole derivatives. The red part represents the tetrazole ring or pyrazine ring.

Finally, the volatiles were eliminated under low pressure, then the residue was purified using 10% ethyl acetate/petroleum ether on a silica column to obtain the nitrile-substituted pyrazine (3).

General Procedure for Synthesizing A1-A4

Briefly, nitrile substituted pyrazine (3,1 mmol), sodium azide (1.5 mmol), zinc bromide (2 mmol), and water (2 mL) were put to the 25 mL round-bottomed flask, then vigorously stirred for 12 h. Next, cool the solution to room temperature, then tetrazole was isolated via filtration, cleaned with 3 N hydrogen chloride (HCl) and air-dried in a drying oven to obtain the product (A1-A4). Then, the final products A1-A4 were collected, and their purity was validated by proton nuclear magnetic resonance (^{1}H NMR; ≥ 95%).

General Procedure for Synthesizing B1-B7

Briefly, nitrile substituted pyrazine (3, 1 mmol), sodium azide (1.5 mmol), zinc bromide (2 mmol), and water (2 mL) were put to the 25 mL round-bottomed flask, vigorously stirred for 12 h. Cool the solution to room temperature, then tetrazole was isolated via filtration, cleaned by 2×10 mL 3 N HCl, and air-dried in the drying oven to obtain products B1–B7 (white or slightly colored powder). The final products B1-B7 were collected, and their purity was confirmed by ^{1}H NMR (≥ 95%).

Nuclear Magnetic Resonance

^{1}H NMR spectra were recorded with dimethyl sulfoxide (DMSO) on a 400 MHz spectrometer. The chemical shifts of protons are reported as 0.0001% downfield of tetramethylsilane (TMS) using the residual protium in the NMR solvent as the reference (DMSO = δ 2.50 ppm). Carbon nuclear magnetic resonance (^{13}C NMR) spectra were recorded with DMSO on a 101 MHz spectrometer. The chemical shifts of carbon are reported as 0.0001% downfield of TMS using the carbon resonance of the residual peak as the reference (DMSO = δ39.6 ppm). The NMR data: chemical shift (δ ppm), multiplicity (s = singlet, d = doublet, t = triplet, q = quartet, m = multiplet, br = broad), coupling constant in Hertz (Hz), and integration.

Cell Culture

NCM460 (Human, CRL-1831, ATCC), HCT116 (Human, CCL-247, ATCC), SW480 (Human, CCL-228, ATCC), and CT26 (Mouse, CRL-2638, ATCC) cell lines were grown in Dulbecco modified Eagle medium (DMEM; Gibco, Gaithersburg, MD, USA) with 10% fetal bovine serum and 1% penicillin/streptomycin (Gibco, USA) at 37°C and 5% CO_2 in an incubator (WIGGENS, Germany).

Cell Counting Kit-8 Assay

The Cell Counting Kit-8 (CCK-8; Dojindo, Kumamoto, Japan) was used to evaluate the viability of CRC cells after treatment with compounds which concentrations were various. Briefly, 7×10^3 NCM460, HCT116 and SW480 cells/well were cultivated overnight by a 96-well plate (Thermo science, Waltham, MA, USA). Next, the cells were treated with appropriate 5-fluorouracil, Hydroxyurea, Phenazine, Valsartan, A1-A4, and B1-B7 concentrations for the indicated times. Next, the CCK8 solution (10 μL) was added and incubated at 37°C for 1 h. Then, a microplate reader was used to measure the optical density (OD) at 450 nm (TECAN, infinite M 200 PRO; Tecan, Switzerland). The reported data are from at least three independent experiments.

Evaluation of Cellular Uptake of B7 by CRC Cells

Briefly, 7×10^3 NCM460, HCT116 and SW480 cells/well were cultivated overnight by a 96-well plate (Thermo science, USA). Next, cells were treated with phosphate buffered saline (PBS) or 5-fluorouracil, Hydroxyurea, Phenazine, Valsartan, A1-A4, B1-B7 for 24 h. The full-band wavelengths (TECAN, infinite M200PRO, Switzerland) of PBS-treated cells (termed the PBS group), 5-fluorouracil-treated cells (termed 5-fluorouracil group), Hydroxyurea-treated cells (termed Hydroxyurea group), Phenazine-treated cells (termed Phenazine group), Valsartan-treated cells (termed Valsartan group), A1-A4-treated cells (termed A1-A4 group), B1-B7-treated cells (termed B1-B7 group) were measured, and the

298 nm wavelength was selected for further uptake assays. Next, to measure the cellular uptake of 5-fluorouracil, Hydroxyurea, Phenazine, Valsartan, A1-A4, B1-B7 by CRC cells, OD values of PBS-treated cells, 5-fluorouracil-treated cells, Hydroxyurea-treated cells, Phenazine-treated cells, Valsartan-treated cells and A1-A4, B1-B7-treated cells at 298 nm were measured at 0, 4, 8, 12, 20, 24 h, and data were analyzed by GraphPad Prism 5 Software (USA).

Flow Cytometry

1.2×10^6 HCT116 and SW480 cells/well were cultivated overnight by a 6-well plate (Thermo science, USA). Next, cells were treated with B7 for 24 h. The cells (1×10^6 / mL) were collected and washed, then stained with a mixture of Annexin V-fluorescein isothiocyanate/propidium iodide for 30 min. Cell fluorescence analysis used the flow cytometer (BD BIOSIS, USA).

TUNEL Assays

2×10^4 HCT116 cells/well were cultivated overnight by a 24-well plate (Thermo science, USA) with coverslips. After incubation with B7 for 24 h, cells were fixed with 4% paraformaldehyde (PFA) for 30 min, washed and stained with terminal deoxynucleotidyl transferase dUTP nick end labeling (TUNEL) reagent (Promega, g3250) for 20 min. Hoechst 33,342 (10 ng/mL, Thermo science, USA) was used for nuclei visualization. The apoptotic and non-apoptotic signals were obtained by DM 2500 fluorescence microscope (Leica, Germany).

RNA Isolation and Quantitative PCR

HCT116 or SW480 cells were cultivated overnight by 6-well plates (Thermo Science, USA) and starved in a serum-free medium for 4 h after reaching 80% confluence. Next, two replicates of HCT116, SW620, or SW480 cells were incubated with or without B7 for 24 h before their total RNA was extracted using TRIzol reagent (Invitrogen, Carlsbad, CA, USA). The BioRT cDNA First-Strand Synthesis Kit (Bioer Technology, Hangzhou, China) and BioEasy SYBR Green I Real-Time PCR Kit (Tiangen, Beijing, China) were used for cDNA synthesis and quantitative PCR (qPCR) detection. The reaction began with a hold at 94°C for 3 min, followed by 35 cycles of dissociation at 94°C for 10s, annealing at 59°C for 15s, and extension at 72°C for 30s. The glyceraldehyde 3-phosphate dehydrogenase (GAPDH) gene was used as the internal reference. All primer sequences (including normalization control) for the qPCR are provided in Table 1. The $2^{-\Delta\Delta CT}$ method was used to calculate gene expression levels. All experiments were conducted in triplicate.

Table 1 The Primer Sequences for the qPCR

Gene	Sequence	Amplicon Size	TM (°C)
GAPDH	F: CCATGGGGAAGGTGAAGGTC R: GAAGGGGTCATTGATGGCAAC	113 bp	60.03 59.52
BAX	F: TTTGCTTCAGGGTTTCATCC R: ATCCTCTGCAGCTCCATGTT	162 bp	56.21 59.08
BCL-2	F: GAGGATTGTGGCCTTCTTTG R: GCCGGTTCAGGTACTCAGTC	116 bp	56.69 60.11
Caspase-3	F: TGGAACAAATGGACCTGTTGACC R: AGGACTCAAATTCTGTTGCCACC	244 bp	61.25 61.31
Caspase-9	F: AAGCCAACCCTAGAAAACATTACC R: GACATCACCAAATCCTCCAGAAC	120 bp	59.23 59.31
Caspase-1	F: TACCTCTTCCCAGGACATTA R: ATGGACTTTCAGTACCCTTTC	110 bp	54.52 55.21
Beclin-1	F: TGAAATCAATGCTGCCTGGG R: CCAGAACAGTATAACGGCAACTCC	162 bp	58.81 61.45

(*Continued*)

Table 1 (Continued).

Gene	Sequence	Amplicon Size	TM (°C)
XCT	F: AAGGTGCCACTGTTCATCCC R: TGTTCTGGTTATTTTCTCCGACA	198 bp	60.25 58.04
LC3A	F: GACCGCTGTAAGGAGGTGC R: CTTGACCAACTCGCTCATGTTA	153 bp	60.45 58.67
LC3B	F: GATGTCCGACTTATTCGAGAGC R: TTGAGCTGTAAGCGCCTTCTA	167 bp	58.7 59.45
P62	F: GCACCCCAATGTGATCTGC R: CGCTACACAAGTCGTAGTCTGG	92 bp	59.19 60.73
FTH1	F: GGTGCGCCAGAACTACCAC R: TCGCGGTCAAAGTAGTAAGACATGG	111 bp	61.03 62.84
E-Cadherin	F: GTCTGTAGGAAGGCACAGCC R: TCATCCTCTGGGGGCAGTAA	161 bp	60.39 59.96
N-Cadherin	F: AGAGGCTTCTGGTGAAATCGC R: TGGAAAGCTTCTCACGGCAT	214 bp	60.68 59.96

Western Blotting

HCT116 or SW480 cells were seeded into 6-well plates (Thermo science, USA), starved in a serum-free medium for 4 h after reaching 80% confluence. Next, the cells were cultivated with or without B7 (24 h) before their total proteins were extracted using Beyotime protein extraction buffer (Beyotime, China). The concentration of proteins in CRC cells was detected using a BCA Protein Assay Kit (Chinese Radix Scutellariae, China). After adding a loading buffer, the samples were boiled, and the proteins were separated using sodium dodecyl sulfate polyacrylamide gel electrophoresis (SDS-PAGE). Next, the separated proteins in the gel were transferred to polyvinylidene difluoride (PVDF) membranes (IPVH00010, Merck Millipore, USA) and immunoblotted with 1000 times diluted primary antibodies: anti-caspase-3 (CST, #9662, USA), anti-cleaved caspase-3 (CST, #9664, USA), anti-BAX (CST,#2772, USA), anti-BCL2 (CST,#4223, USA), anti-P53 (Abcam, ab131442, USA), anti-E-Cadherin ((Proteintech, 20,874-1-AP, USA), anti-N-Cadherin (Proteintech, 22,018-1-AP, USA), anti-XCT (CST,#98051, USA), anti-FTH1 (CST,#3998, USA), anti-ALOX15 (Abcam, ab242062, USA), anti- ACSL4 (Abcam, ab155282, USA), anti-GPX4 (Abcam, ab252833, USA), anti-Beclin -1 (CST,#54101, USA), anti-LC3A/B (CST,#4108, USA), anti-P62 (CST,#5114, USA), anti-β-actin (CST,#4967, USA) and anti-GAPDH (Bioworld, AP0066, USA). Then, the membranes were incubated with secondary anti-mouse or anti-rabbit antibodies (Boster, China) conjugated with horseradish peroxidase (HRP) for 1 h and visualized using the Pierce ECL Super Signal Reagent (Thermo Fisher Scientific).

Immunofluorescent Staining

Briefly, the 2×10^4 HCT116 cells/well were cultivated overnight by a 24 well plate (Thermo science, USA) with coverslips. After incubation with B7 for 24 h, cells were immobilized with 4% PFA for 30 min and washed twice with PBS (add 0.2% Triton X-100). Next, the cells were incubated for 1 h in PBS containing 1% bovine serum albumin (BSA) and stained with anti-Caspase-3 (in 1% BSA) antibodies overnight at 4°C. Next, the cells were washed thrice with PBS, stained with Alexa Fluor 488 (Thermo Fisher Scientific) conjugated secondary antibodies for 1 h, followed by 10 ng/mL of Hoechst 33,342 stain for 20 min (Thermo Fisher Scientific). Images were obtained by DM2500 fluorescence microscope (Leica).

Morphological Analysis of Mitochondria

Briefly, 2×10^4 HCT116 cells/well were cultivated overnight by a 24-well plate (Thermo Fisher Scientific). Next, the cells were treated with PBS or B7 for 24 h before being harvested and fixed with 2% PFA for 5 min. Next, the cells were

washed and suspended in a PBS buffer. The cell suspension was loaded onto a mesh and incubated at 37°C for 10 min. Next, electron microscope (EM) mesh surface was stained with 1% uranyl acetate solution for 2 min. Then, the excess uric acid solution was removed from the net using filter paper before it was dried. Mitochondria morphology was observed using a transmission EM (TEM; HT-7800; Hitachi, Japan).

Molecular Docking

The 3D structures of Beclin-1, LC3A, LC3B, and P62 complexed with the small molecule compound B7, Beclin-1 complexed with 5-fluorouracil, hydroxyurea, phenazine and valsartan were computationally predicted to assess their binding affinities. The 3D structures of these proteins were obtained as Protein Data Bank (PDB) files from the UniProt (https://www.uniprot.org/) and PDB (https://www1.rcsb.org/) databases. The water molecules, unrelated protein chains, and original ligands were deleted from these protein structures before docking using PyMOL (v.2.3.0) software. The small molecular compounds were B7, 5-fluorouracil, hydroxyurea, phenazine and valsartan. There 3D structures were obtained as a Structure-Data File (SDF) from the ChemicalBook database. It underwent MMFF94 molecular force field optimization using Chem3D (v.2020) software to obtain the optimal molecular structure.

Molecular docking was performed by AutoDockTools (v.1.5.6) software to hydrogenate proteins and small molecules and determine reversible bonds. Grid plate was used to set the molecular docking range parameters, the docking mode was set to semi-flexible docking, and the docking algorithm was set to the Lamarckian genetic algorithm. AutoDockVina (v.1.2.0) was used for molecular docking and to obtain the docking binding free energy and docking result file. A molecular binding energy of < 0 kcal mol^{-1} means that receptors and ligands can bind spontaneously without external energy, the binding energy of < -7 kcal mol^{-1} represents strong binding. PyMOL (v.2.3.0) and DiscoveryStudio (v.2019) software were used to visualize the results.

Cell Migration Analysis

Briefly, 5×10^5 HCT116 and SW480 cells/well were cultivated overnight by a 6-well plate. Next, cells were treated with PBS or B7 for 24 h. After scraping, cells were further cultured using a serum-free medium. Cell migration scratch regions were observed at 0, 24, and 48 h using an inverse microscope, and the cell migration area was analyzed using the ImageJ software. All experiments were conducted in triplicate.

Cell Invasion Analysis

HCT116 and SW480 cells were treated with either PBS or B7 for 24 h. Next, 3×10^4/well PBS-treated or B7-treated HCT116 and SW480 cells were put to the upper transwell chambers (Corning, New York, USA) containing 100 µL of Matrigel (BD Biosciences, Franklin Lake, NJ, USA). The medium (DMEM) with 10% fetal bovine serum was fed into the lower room (Corning, New York, USA). After incubation at 37°C for 24 h, cells that had moved to the bottom of the membrane were fixed using 4% PFA and stained with 0.1% crystalline purple dye (Solarbio, Beijing, China). The staining cells were counted by reverse microscopy and analyzed using ImageJ software. All experiments were conducted in triplicate.

Animals and Animal Care

The BALB/c mice (n = 26, 50% male, eight weeks old) were got from the Laboratory Animal Center of Jilin University (Changchun, China). They were housed in laboratory cages under 50–60% relative humidity, a 12/12 h light/dark cycle, and specific pathogen-free conditions and provided standard rodent foods and drinking water. All operations were performed under sterile conditions. Each mouse was subcutaneously injected with CT26 cells (1×10^6) in their left flank, and tumor growth was observed after seven days. Drug verification was conducted once the tumor volume reached 100–150 mm^3. The mice were casually divided into five groups (n = 5). One was administered PBS (negative control) for 21 days, and three were administered different B7 concentrations (0.275, 0.55, or 1.375 mg/kg) for 21 days. A positive control group was administered 5-fluorouracil (1 mg/kg) for 21 days. The tumors' length (L) and width (W) were recorded daily, and their volumes were calculated as $L\times W^2/2$. The mice's body weight and status were monitored daily. If rapid loss of 15–20% of the original body weight, loss of appetite and weakness, infection of body organs, the tumor

grows more than 10% of the animal's original body weight, the tumor volume exceeds 150 mm^3 and ulceration of tumors occur in the process, euthanasia should be carried out immediately. The mice to be euthanized were placed in the small animal anesthesia room, and the mice were anesthetized with 0.41 mL/min at 4 L/min Fresh gas flow (2%) isoflurane general anesthesia. After anesthesia, a deep pain test was carried out and fingers were used to squeeze the animal's hindlimb toes. If the animal did not respond to the test, it was unconscious or disappeared, and the anesthesia met the requirements, followed by cervical spine dislocation and execution. Above 5 min, there is no breath, no heartbeat, nerve reflex disappears, corneal reflex disappears, pupil dilates, and animal death can be verified. All animal studies were approved of the Laboratory Animal Ethics Committee of Jilin University, China (approval number: SY202109003).

Hematoxylin-Eosin (H&E) Staining

On day 22, tumor tissues were harvested, dehydrated, and embedded in paraffin. Then, 5-μm-thick paraffin sections were cut, stained with hematoxylin and eosin (H&E), air-dried, and visualized under a microscope (Olympus, Japan).

TUNEL Assays of Tumor Tissue

Moisture was removed from paraffin section with xylene and ethanol. Next, the section was incubated with proteinase K at 37°C for 30 min before adding 50 μL of TUNEL reaction solution. Then, 4′,6-diamidino-2-phenylindole dye solution was added. Finally, the sections were imaged using a DM 2500 fluorescence microscope (Leica, Germany).

Ki-67 Assessment

The tissue sections were placed in a repair box filled with EDTA antigen repair buffer (PH 9.0) (Yiyuan, Changchun, China) for antigen repair in microwave oven. Add 3% BSA to incubate 30 min at room temperature. Remove the sealing solution, add 1:600 diluted Ki- 67 monoclonal antibody (Abcam, ab15580, UK) to the slices, and incubate overnight in a wet box at 4°C. The glass slides were placed in PBS (PH 7.4) and shaken and washed on the decolorizing shaker. After the slices were dried, secondary anti-mouse antibodies (Boster, China) was added to cover the tissue, and 50 min was incubated at room temperature. The slices were cleaned with PBS and dried with DAB chromogenic agent (Shitai, Nanjing, China), and the color was controlled by microscope (Leica, Germany).

Statistical Analysis

Differences between pairs of groups in CCK-8 detection, apoptosis, migration, invasion, qPCR, and tumor volume were evaluated using the unpaired Student's *t*-test. Data are presented as mean ± standard deviation (SD). Statistical analyses were performed using GraphPad Prism 5.0 software. Statistical significance is indicated as: *$p < 0.05$; **$p < 0.01$; ***$p < 0.001$; ****$p < 0.0001$.

Results

Compound Synthesis and Characterization of B7

The tetrazole-substituted pyrazine compounds were synthesized using the novel chemoenzymatic method described in Figure 2. Pyrazine ring 3 was obtained from diaminomaleonitrile 1 with α-diazo-β-carbonyl compounds based on a hemoglobin catalyzed carbene-transfer reaction. Sodium azide was added to nitrile to synthesize tetrazole-substituted pyrazine compounds A1-A4 and B1-B6 to obtain ^{1}H-tetrazoles. In addition, the target compound B7 was prepared by cycloaddition of sodium azide and intermediate 3 (R_2 = COOMe) with concomitant R2 hydrolysis. The compound structures were examined using ^{1}H NMR, ^{13}C NMR, and HRMS spectra, and these data are provided in Supporting Information (Figure 2 and Data S1). The purity of all target complexes was ≥95%.

Effects of B7 on CRC Cell Proliferation and Apoptosis

NCM460, HCT116, and SW480 cells were treated with 5-fluorouracil (2, 4, 6, 8, and 10 μM) and hydroxyurea (10, 20, 30, 40, and 50 μM) for 24 h. CCK-8 results suggested that 5-fluorouracil and hydroxyurea could inhibit CRC cell growth and were toxic to normal human colorectal epithelial cells NCM460 (Figure S1A–C). Then, NCM460, HCT116, and

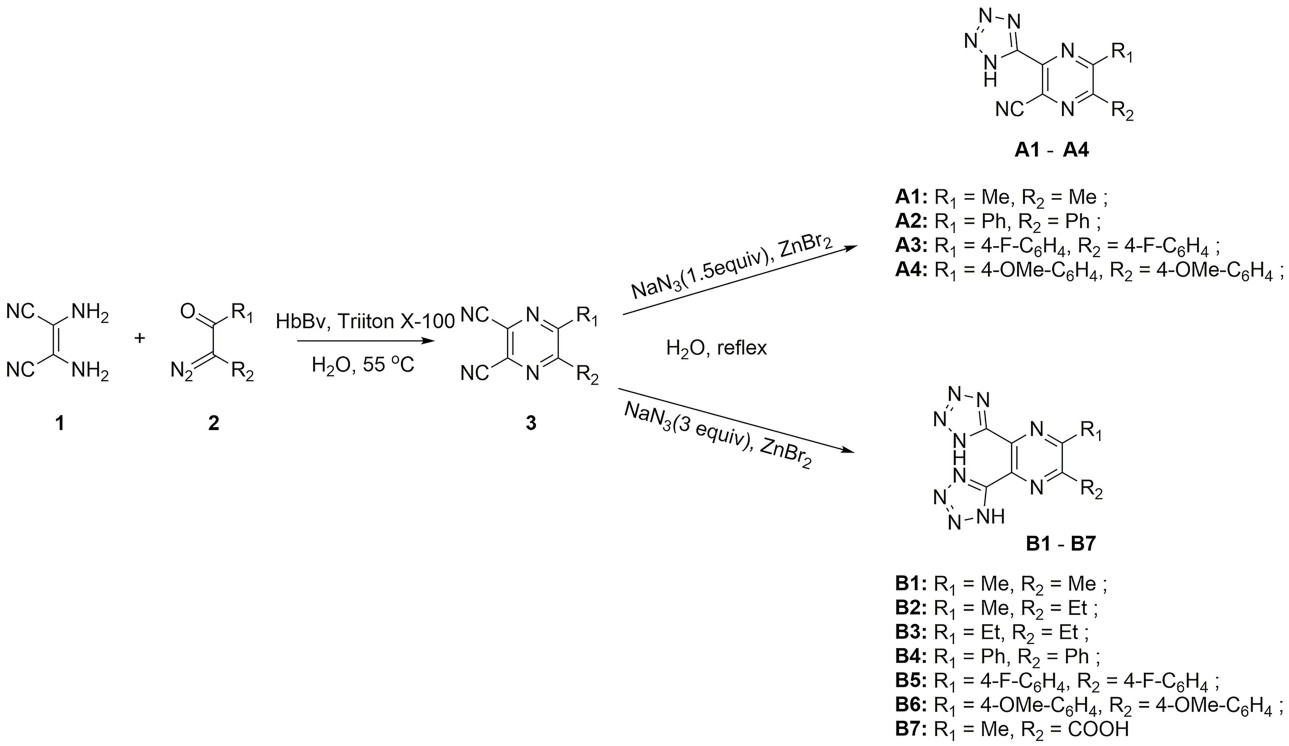

Figure 2 Chemoenzymatic synthesis of tetrazole-substituted pyrazine compounds.

SW480 cells were incubated with phenazine (1, 5, 10, 15, and 20 μM) and valsartan (10, 20, 30, 40, and 50 μM) for 24 h. The CCK-8 results showed that they had no significant inhibitory effects on CRC cells (Figure S1A–C). In addition, to explore the uptake of drugs and compounds in cells, we first explored the full-band wavelength of PBS-treated cells, selecting the 298 nm wavelength for uptake experiments. Figure S1D shows that absorbance at 289 nm increased with incubation time, indicating that NCM460, HCT116, and SW480 cells effectively absorbed the drugs and compounds throughout the 24 h.

To confirm whether the synthesized compounds could inhibit CRC cell proliferation, NCM460, HCT116, and SW480 cells were treated with A1-A4 and B1-B7 compounds (0.2, 0.4, 0.6, 0.8, and 1 μM) for 24 h. The CCK-8 results showed that compounds A1-A4 and B1-B6 had negligible inhibitory effects on CRC cell growth (Figures 3A and B, S2A). In contrast, compound B7 inhibited CRC cell growth at concentrations from 0.4 to 1 μM (Figure 3C) and was less toxic to NCM460 cells (Figure S2B). Moreover, Figures 3D, S2B and S3 show increasing absorbance at 289 nm with incubation time, indicating that compounds A1-A4 and B1-B7 were effectively taken up by NCM460, HCT116, and SW480 cells throughout the 24 h.

Next, we investigated the cancer cell-killing effects of compound B7 in vitro. The cell apoptosis assay results showed that 12.72% ± 2% of HCT116 cells (Figure 4A and B) and 16.59% ± 2% of SW480 cells (Figure S4A and B) were dead (including early apoptotic, late apoptotic, and necrotic cells) after incubation with 0.4 μM of B7 for 24 h. The apoptosis of CRC cells after B7 treatment was further confirmed by TUNEL analysis (Figures 4C and D, S4C and D). The expression levels of critical apoptosis-associated genes after B7 treatment were then explored. Figure 4E shows that the mRNA level of Caspase-3 increased significantly after B7 treatment, while those of *BCL*$_2$ and *BAX* did not change significantly (Figures 4E and S4E). Similarly, protein levels of Caspase-3 and cleaved Caspase-3 increased significantly after B7 treatment, while those of BCL_2 and BAX did not change significantly (Figures 4F and H, S4F and H). Altogether, these results indicate that B7 could induce CRC cell apoptosis by increasing Caspase-3 mRNA and protein levels.

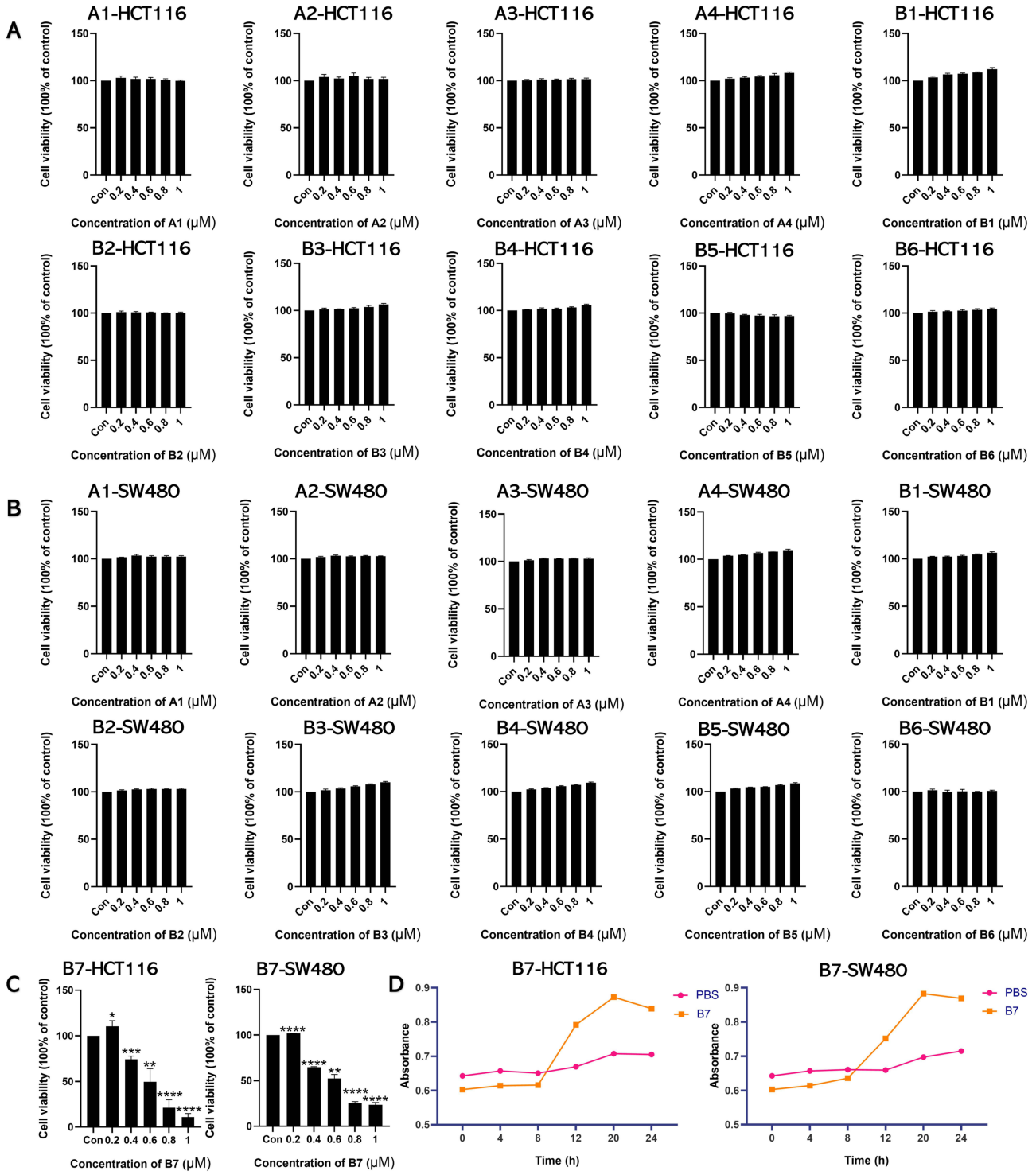

Figure 3 Intracellular uptake of B7 inhibits CRC cell proliferation. (**A**) CCK-8 assay showed the effects of A1-A4 and B1-B6 on HCT116 cells. (**B**) CCK-8 assay showed the effects of A1-A4 and B1-B6 on SW480 cells. (**C**) CCK-8 assay was utilized to measure the effect of B7 on proliferation. (**D**) The uptake of B7 in HCT116 and SW480 cells over time. The data are represented as the mean ± SD (n = 3). Statistical differences were considered significant at *p < 0.05, **p < 0.01, ***p < 0.001 and ****p < 0.0001.

Effects of B7 on Autophagy and Ferroptosis in CRC Cells

Autophagy, one of the most important types of programmed cell death, has beneficial and detrimental effects in tumorigenesis. Autophagy can inhibit the activation of oncogenes and prevent tumorigenesis.[28] However, in malignant, transformed cancer cells, autophagy provides nutrients for the survival of cancer cells through promoting the

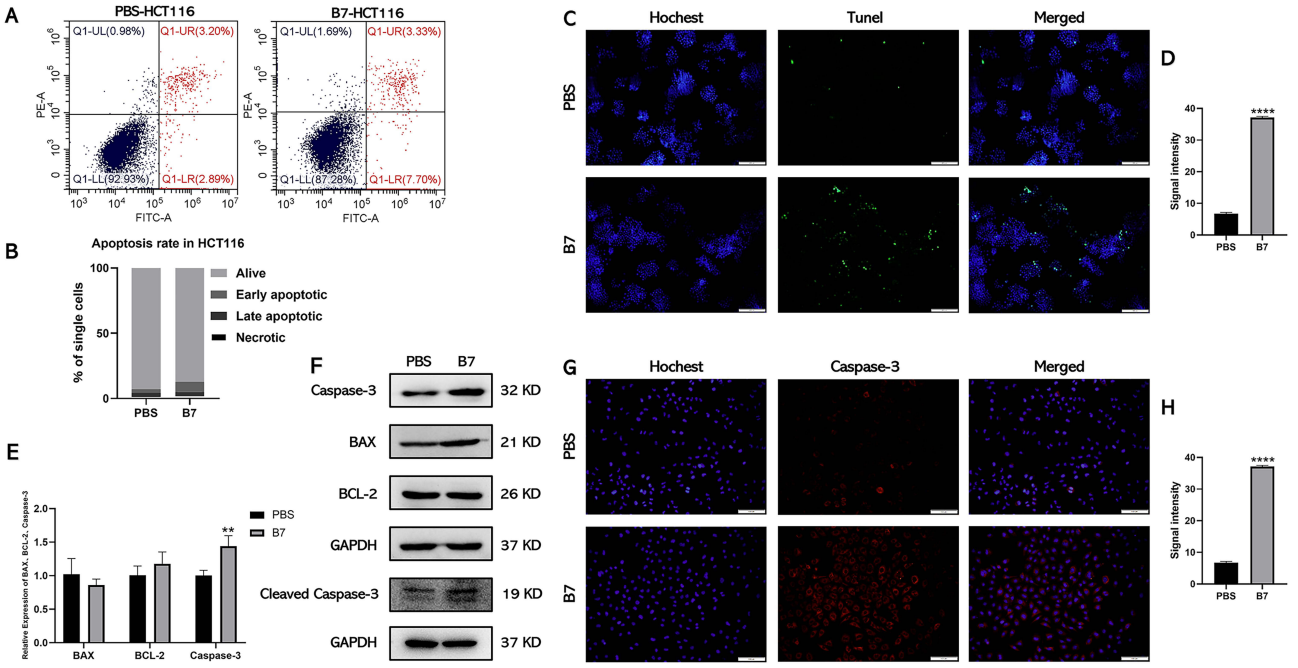

Figure 4 B7 induces apoptosis of CRC cells by promoting the expression of Caspase-3. (**A**) Flow cytometry was used to analyze the effect of B7 on HCT116 cell apoptosis. (**B**) Statistical analysis of the percentage of HCT116 cells undergoing apoptosis. Statistical significance be-tween groups were evaluated using the Student's *t*-test for independent groups. (**C**) TUNEL analysis of HCT116 cells treated with B7 (scale bar = 100 μm). And associated (**D**) statistical analysis of TUNEL fluorescence signal intensity. (**E**) Relative gene expression of apoptosis-related genes in HCT116 cells treated with PBS or B7. (**F**) Protein levels of BCL-2, BAX, Caspase-3, cleaved Caspase-3 and GAPDH in HCT116 cells treated with PBS or B7. (**G**) The fluorescent images of Caspase-3 in HCT116 cells treated with PBS or B7 (scale bar = 100μm). And associated (**H**) statistical analysis of the Caspase-3 intensity. The data are represented as the mean ± SD (n = 3). Statistical differences were considered significant at **p < 0.01 and ****p < 0.0001.

proliferation, invasion, and metastasis of malignant tumors.[29] The effects of B7 on autophagy in CRC cells were assessed by exploring their mitochondrial morphology using TEM. Unlike PBS-treated cells, B7-treated cells showed mitochondrial pyknosis, vacuolation, and membrane rupture (Figure 5A), indicating autophagy suppression.

In addition, qPCR was used to examine the expression of autophagy-related (*LC3A/B, P62*, and *Beclin-1*) and ferroptosis-related (*XCT* and ferritin heavy chain 1 [*FTH1*]) genes since autophagy is usually accompanied by iron death. After treatment with B7, the expression of *Beclin-1* decreased significantly, while that of other autophagy genes did not change significantly (Figures 5B and C, S5A and C). Western blotting confirmed that B7 treatment decreased the Beclin-1 protein level (Figure 5D) but had no effect on autophagy-related proteins LC3A/B and P62 or ferroptosis-related proteins ALOX15, ACSL4, and GPX4 (Figures 5D, S5B and D).

The binding ability of autophagy-associated proteins to B7 was explored using molecular docking. Beclin-1, LC3A, LC3B, and P62 were selected for mapping and force analysis with compound B7. Compound B7 had a binding energy of −8.1 kcal ·mol^{-1} with Beclin-1, −7.0 kcal mol^{-1} with LC3A, −7.1 kcal mol^{-1} with LC3B, and −6.0 kcal mol^{-1} with P62 (Figure S6). The binding energy of B7 with Beclin-1 was <−7 kcal mol^{-1}, indicating strong binding. Moreover, the types of forces formed were rich, and the number of acting bonds was considerable. B7 interacts with amino acid residues LEU-440 and VAL-269 in the A chain of Beclin-1 protein to form two Alkyl/ π-Alkyl bands, and forms three conventional hydrogen bonds with THR-273, ALA-272 and SER-444 of A chain, thus the binding of B7 to Beclin-1 is likely to play a corresponding role. In addition, Beclin-1 was selected for mapping and force analysis of compounds 5-fluorouracil, hydroxyurea and phenazine and valsartan. The binding energies of Beclin-1 to compound 5-fluorouracil, hydroxyurea, phenazine and valsartan are −5 kcal mol^{-1}, −4.3 kcal mol^{-1}, −6.7 kcal mol^{-1} and −7.3 kcal mol^{-1} (Figure S7). The binding energies of the four compounds were <0 kcal mol^{-1}, which confirmed that the four compounds could bind to Beclin-1 spontaneously. Therefore, B7 suppressed autophagy in CRC cells by regulating Beclin-1 expression but had no significant effect on ferroptosis.

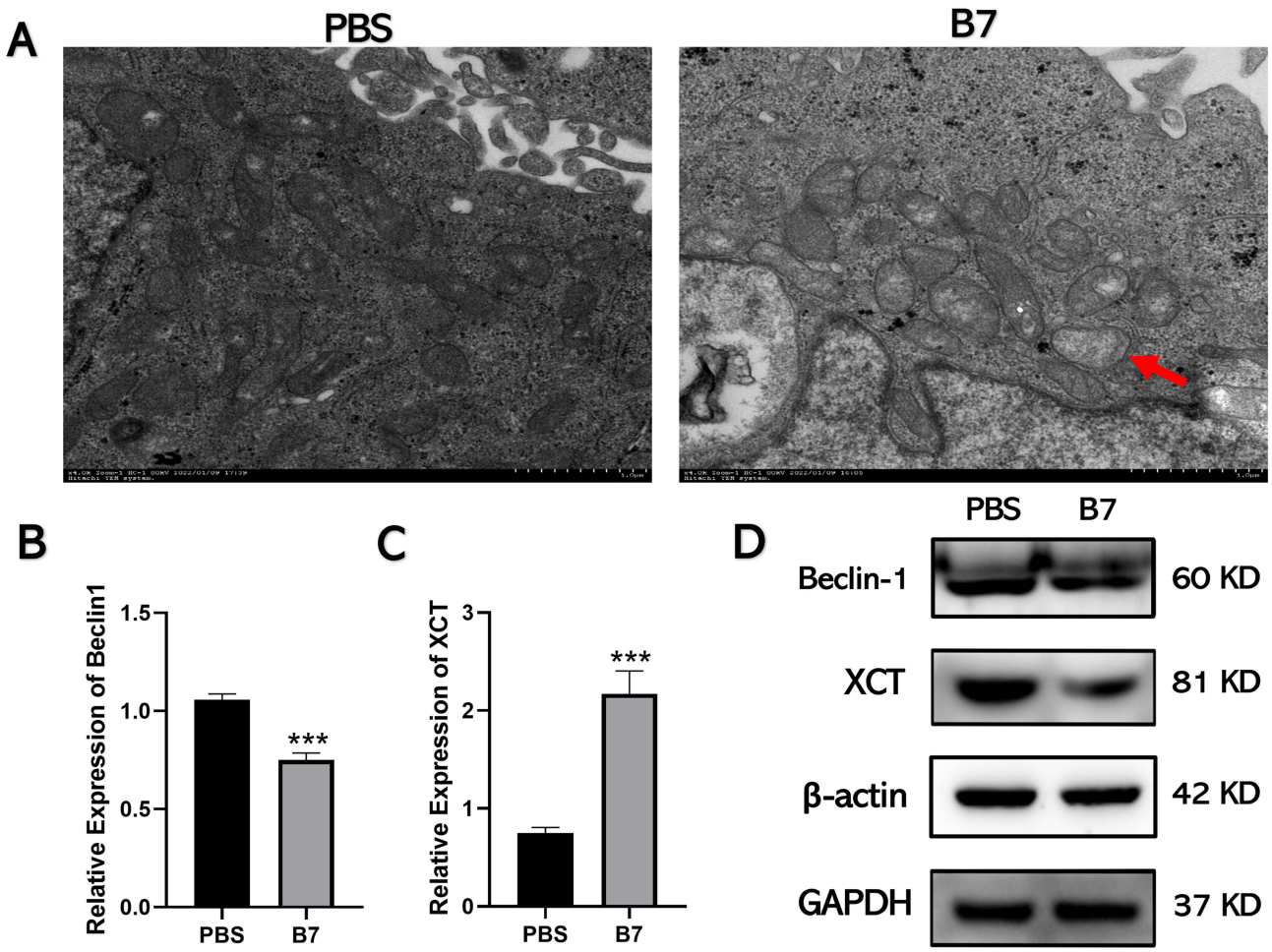

Figure 5 B7 inhibits autophagy of CRC cells by inhibiting Beclin-1. (**A**) The morphology of mitochondria was observed by transmission electron microscope. The red arrow indicated that mitochondria in group B7 showed pyknosis, vacuolation, and membrane rupture. (**B**) The expression of the autophagy-related gene *Beclin-1* was detected by qPCR. (**C**) The expression of the ferroptosis-related gene *XCT* was detected by qPCR. (**D**) Expression levels of XCT, Beclin-1, and GAPDH proteins were assessed via Western blotting. The data are represented as the mean ± SD (n = 3). Statistical differences were considered significant at ***p < 0.001.

Effects of B7 on CRC Cell Migration and Invasion

The effects of B7 on CRC cell migration and invasion were examined using the cell wound healing test and transdermal analysis, respectively. The migration assay results showed reduced migration of B7-treated cells compared to passage-matched normal HCT116 and SW480 cells (Figure 6A and B). Transdermal analysis showed that B7 suppressed CRC cell invasion (Figure 6C and D). In addition, HCT116 and SW480 cells were treated with B7 compounds (0.4, 0.6 and 0.8 μM) for 48 h, and the sublethal dose of B7 was tested in the cell migration assays (Figure S8). During migration and invasion, cancer cells usually lose epithelial markers, such as E-Cadherin, and develop increased N-Cadherin levels. Therefore, the mRNA and protein levels of E-Cadherin and N-Cadherin were examined. The results showed that E-Cadherin was increased, and N-Cadherin expression was inhibited in B7-treated cells (Figure S5E and F), indicating that B7 might inhibit CRC cell metastasis by suppressing CRC migration and invasion.

B7 Inhibits the Growth of Colorectal Tumors in vivo

The antitumor activity of B7 in vivo was evaluated by constructing a colorectal xenograft model. Figure 7A shows that the chemotherapeutic drug 5-fluorouracil had the strongest inhibitory effects on CRC tumor growth as a positive control. Moreover, CRC tumor-bearing mice receiving different B7 concentrations had a reduced tumor burden compared to the uncontrolled tumor growth in PBS-treated mice. Among these treatments, 2 μM of B7 provided statistically significant tumor inhibition compared to PBS treatment, while increasing the B7 dose to 4 or 10 μM further improved its tumor

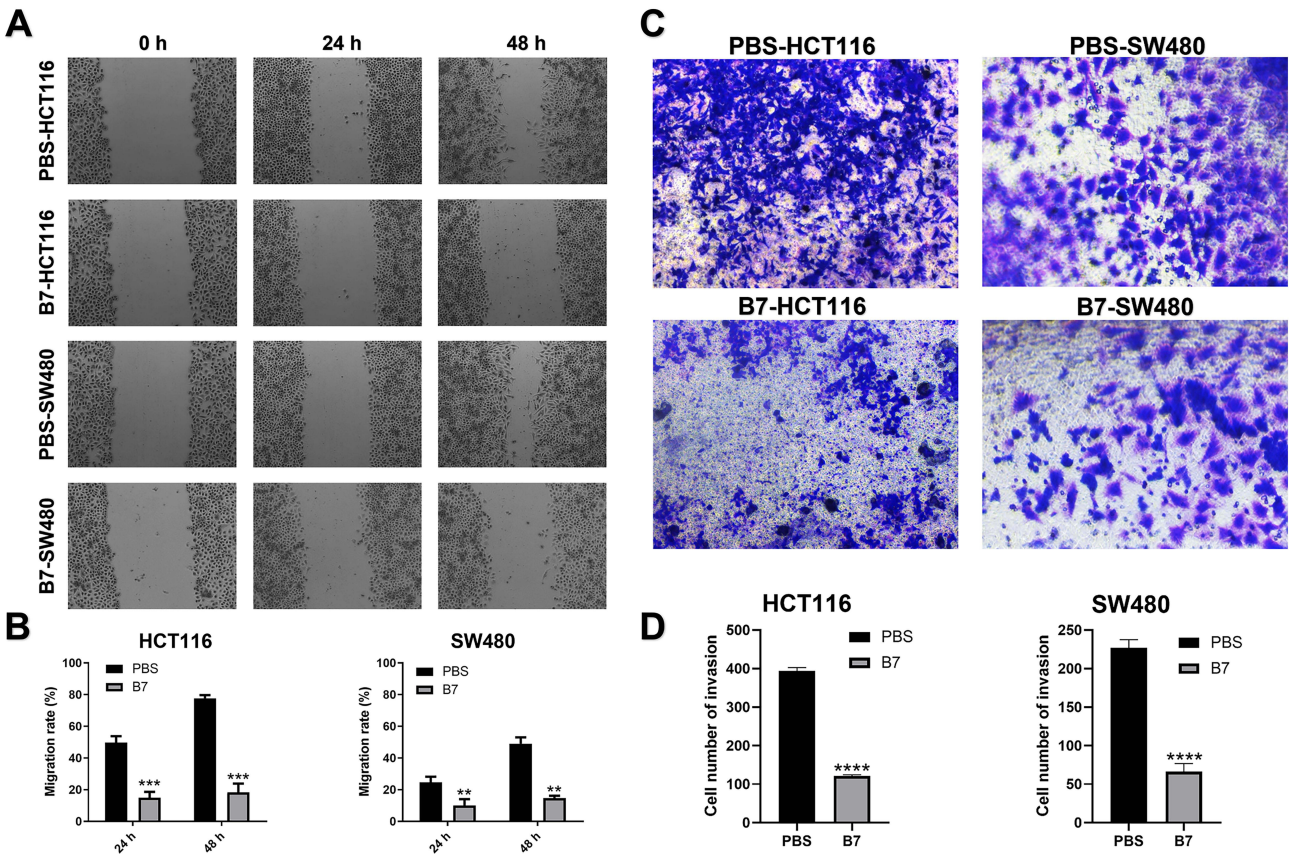

Figure 6 B7 inhibits the migration and invasion of CRC. (**A**) Wound-healing assay images (100× magnification) from HCT116 and SW480 cells treated with PBS and B7. (**B**) Statistical analysis of cell migration. (**C**) Representative transwell invasion assay images (100× magnification) from HCT116 and SW480 cells treated with PBS and B7. (**D**) Statistical analysis of cell invasion. The data are represented as the mean ± SD (n = 3). Statistical differences were considered significant at $^{**}p < 0.01$, $^{***}p < 0.001$, $^{****}p < 0.0001$.

regression effects. However, tumor inhibitory efficiency did not differ significantly between the 4 and 10 μM B7 treatment groups (Figure 7B).

Body weight can provide indirect evidence for treatment toxicity. Figure 7C shows that body weight did not differ significantly between the PBS group and the 2 and 4 μM B7 groups but did between the PBS group and the 10 μM B7 group, indicating that appropriate B7 doses are tolerated and safe (Figure 7C). Furthermore, H&E, TUNEL, and Ki-67 staining showed no apparent pathological changes in the main organs, while more tumor cell damage was observed in the tumors of tumor-bearing mice treated with 4 μM B7 (Figure 7D–G). The mice did not show abnormal weight loss, loss of appetite and weakness, infection of body organs, or tumor rupture during the treatment of each drug. Altogether, our in vivo data suggested B7 could effectively suppress CRC tumor growth without apparent systemic toxicity at a concentration <4 μM.

Discussion

Current studies have shown that many small molecular compounds are promising in cancer therapy.[30] However, there are no effective small molecular compounds for treating CRC. Therefore, we focused on the chemical enzymatic synthesis of tetrazolium-substituted pyrazine compounds and evaluated their anti-CRC effect in vitro and in vivo. The compounds were synthesized using a new chemical enzyme method and designed to contain 1–2 tetrazole rings, a variable group (R1 or R2), and an essential functional pyrazines moiety. To establish the structure-activity relationship (SAR) of pyrazine tetrazole compounds in inhibiting CRC cell growth, we analyzed the effects of the variable group attached to the pyrazine ring (mono- or di-tetrazole ring).

Since tetrazoles inhibit tumor cells most prominently,[14–18] additional bis-tetrazole ring analogs (B1-B7) were synthesized. In addition, compounds with a carboxyl substitution on the pyrazine ring showed increased CRC growth inhibition, likely due to increased water solubility of the whole compound.[11] In conclusion, the results of the A1-A4 and B1-B7 compounds showed that

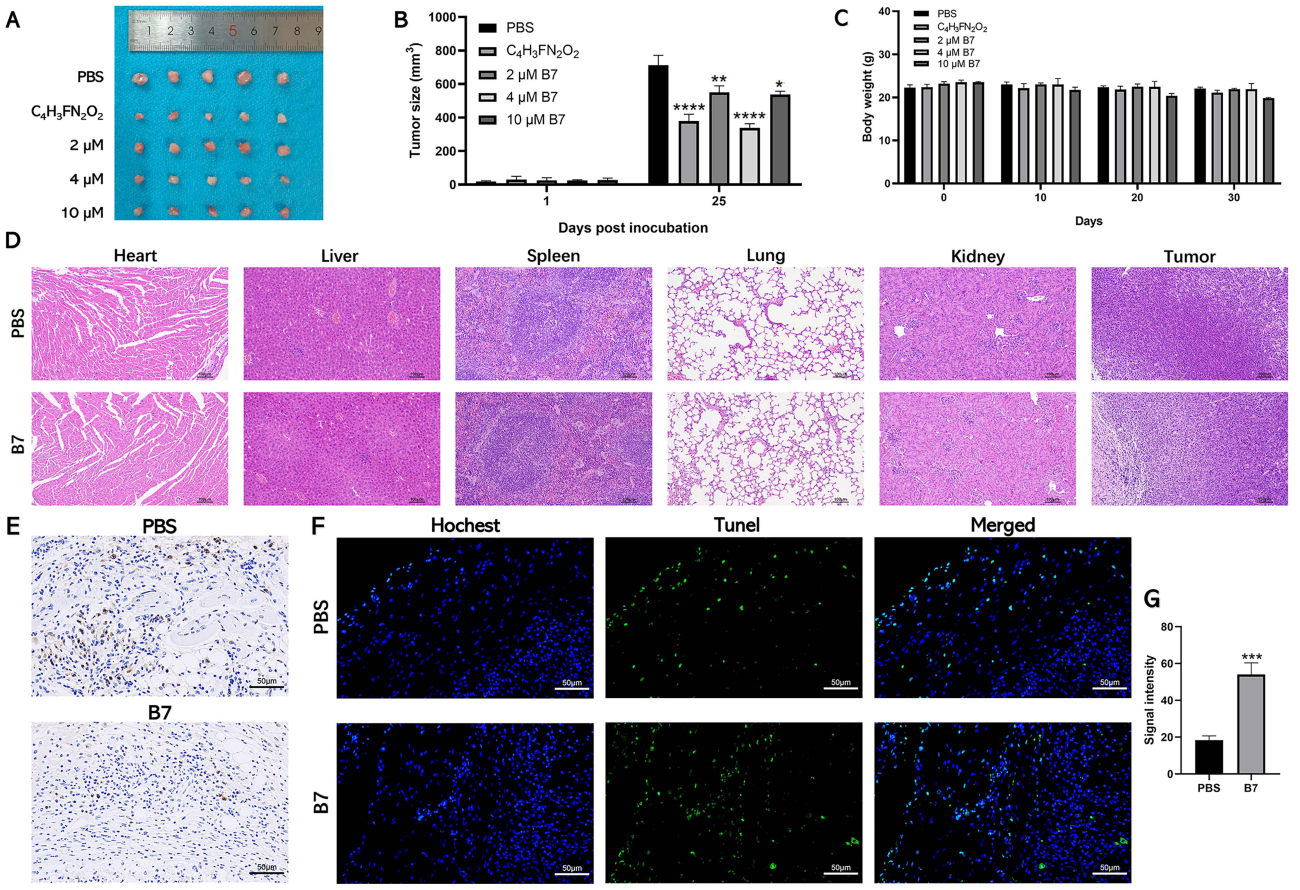

Figure 7 Therapeutic efficacy of B7 against subcutaneous CT26 tumors in vivo. (**A**) Morphological observation of the mouse CRC tumor tissue of different groups. (**B**) The tumor growth curves of CT26 tumor-bearing mice. (**C**) The body weight changes of mice were recorded. (**D**) H&E staining of main organs of mice. The data are represented as the mean ± SD (n = 3). (**E**) Immunohistochemical staining of Ki-67 in tumor tissue. (**F**) TUNEL analysis of H tumor tissue treated with B7 (scale bar = 100 μm). And associated (**G**) statistical analysis of TUNEL fluorescence signal intensity. Statistical differences were considered significant at * $p < 0.05$, ** $p < 0.01$, *** $p < 0.001$, and **** $p < 0.0001$.

pyrazine-containing di-tetrazole ring substitutions with "small alkyl side chains" and a "carboxyl group" exhibited excellent effects on tumor growth inhibition.

Previous studies have confirmed that curcumin analogue MS13, a diarylpentane compound, has been proved to have anti-tumor activity which has cytotoxicity, anti-proliferation and pro-apoptotic activity on SW480 and SW620 cells.[31] Resveratrol can also inhibit proliferation and migration of HCT-116 cells and induce apoptosis.[32] Studies have confirmed that caspase-3 is a prognostic marker in patients with metastatic CRC and is closely related to CRC cell apoptosis.[33] To confirm the inhibitory ability of compound B7 on CRC progression, the effects of proliferation and apoptosis in CRC cells were analyzed in the present study. Our results showed that B7 could inhibit the proliferation of CRC cells without obvious toxic effect on normal colorectal epithelial cells. Moreover, the results suggested that B7 can induce the apoptosis through Caspase-3 in CRC cells. Many studies have shown that Caspase-3 participates in numerous regulatory mechanisms and is closely related to apoptosis pathways.[34–36] Caspase-3 is a central death protease in the apoptotic cascade and catalyzes the specific degradation of many key site proteins.[37,38] Therefore, it plays an irreplaceable role in the apoptosis cascade and is considered the executor and terminator of most apoptosis pathways.[39] Moreover, this study confirmed the effect of B7 treatment on the expression of caspases-1 and caspases-9, and there was no apparent effect (Figure S5G).

Since autophagy and apoptosis are the main types of eukaryotic regulatory cell death, most CRC treatment strategies focus on affecting apoptosis and autophagy to weaken tumor growth.[40] Autophagy is a process in which lysosomes degrade excess proteins after organelle damage to maintain the dynamic balance of cells under stress.[41] Many studies have revealed that autophagy is related to apoptosis.[42,43] Small molecular compounds have targeted the regulation of apoptosis and autophagy, indicating that they have therapeutic potential in developing anticancer drugs.[44] Some studies have confirmed that F1012-2-induced apoptosis is enhanced by autophagy inhibition.[45] A new type of 1,2,4-triazine sulfonamide derivative has been proved to have anti-cancer

activity against CRC cells which can induce apoptosis through endogenous and exogenous pathways, and affect the expression of Beclin-1, thus affecting autophagy.[46] Therefore, the effect of compound B7 on CRC autophagy was explored. The mitochondrial electron microscopy results showed that they were damaged, shrunken, and changed in the B7 group, indicating that autophagy was affected.[47] A previous report indicated that *Beclin-1* is an autophagy regulator linking autophagy to apoptosis, confirming our data.[48] Studies have shown that overexpression of Beclin-1 is contacted with reduced survival in patients with CRC treated with adjuvant 5-fluorouracil.[49] While most studies have shown that Beclin-1 can inhibit tumorigenesis, it has also been reported that Beclin-1 can promote tumor cell survival. Beclin-1 expression was significantly higher in primary hepatocellular carcinoma than in normal liver cells,[50] indicating that it may play a positive role in hepatocellular carcinoma development by promoting autophagy. Therefore, by down-regulating Beclin-1 expression, B7 may also inhibit tumor cell development, consistent with our data showing that B7 treatment inhibited Beclin-1 expression, B7 binds to Beclin-1 through Alkyl/ π-Alkyl bands and conventional hydrogen bond, and the binding energy is strong, inhibiting autophagy in CRC cells. Considering whether the morphological changes of mitochondria and the inhibition of autophagy in B7-treated CRC cells are related to ferroptosis, the expression of ferroptosis-related genes were investigated. However, B7 does not affect the expression of ferroptosis-related genes in CRC cells.

The process of migration and invasion is an important part in CRC development.[51] Thus, the role of B7 in migration and invasion of CRC cells were investigated. In the present study, the migration and invasion were inhibited by B7 in CRC cells. The effect of B7 was also investigated using a CRC xenograft model. 5-fluorouracil is used in a variety of chemotherapy regimens for several cancers including CRC.[7,52,53] It has become one of the most widely employed antimetabolite chemotherapeutic agents in recent decades.[54–56] Like 5-fluorouracil, B7 inhibited tumor growth in vivo. In addition, the H&E staining showed no apparent pathological changes in the main organs and body weight did not differ significantly of tumor-bearing mice treated with 4 μM B7. The mice were in good condition and showed no side effects during treatment. The mice showed no abnormal weight loss, loss of appetite or weakness, organ failure or tumor ulcers, and no animals were euthanized before the end of the study. Altogether, a potential working model for B7 is to induce cell apoptosis via Caspase-3 and inhibit autophagy via Beclin-1 in CRC cells, suppressing CRC tumor growth in tumor-bearing mice (Figure 8).

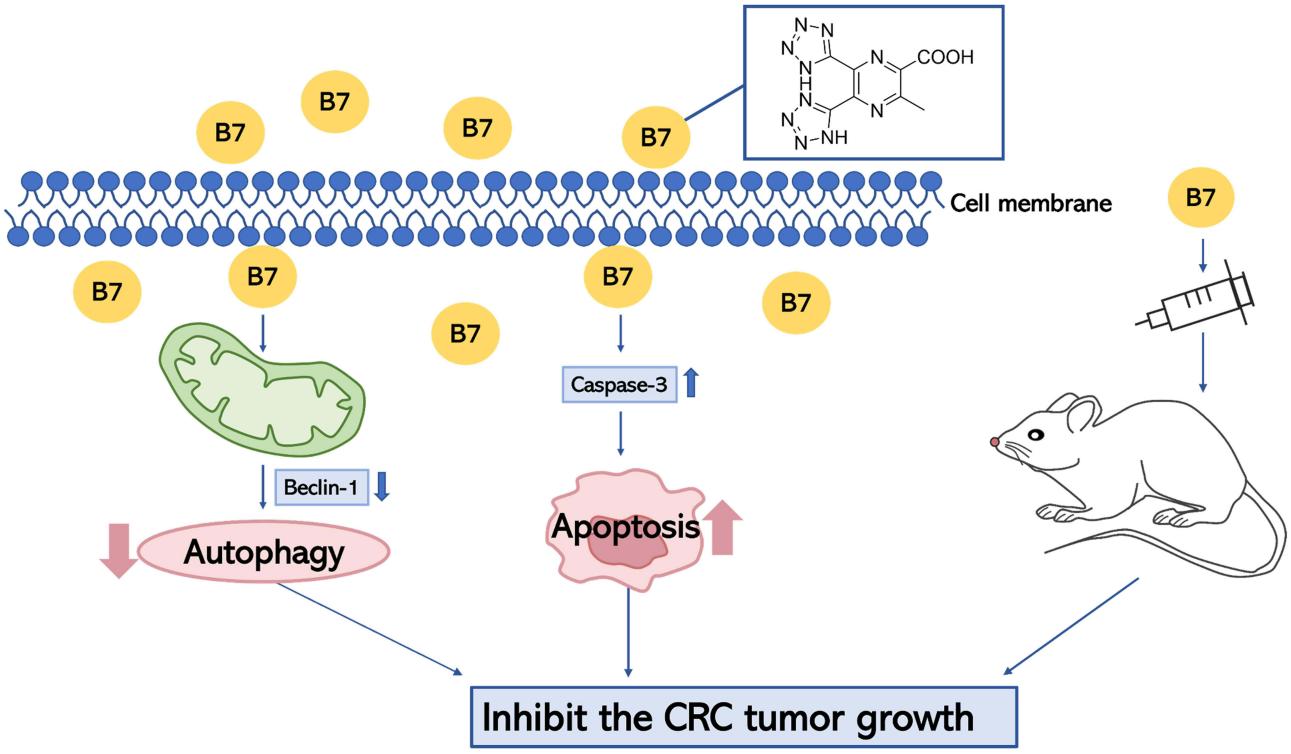

Figure 8 Working model of B7 and its inhibitory role in regulating tumor growth.

Conclusion

In summary, compound B7 was synthesized efficiently using tetrazolium-substituted pyrazine via a chemoenzymatic method. B7 modulated the expression of Caspase-3 which is essential in tumor cell apoptosis in CRC cells, inducing their apoptosis. In addition, B7 treatment decreased Beclin-1 expression, indicating inhibited autophagy. This study showed that B7 effectively inhibited CRC cell proliferation, migration, and invasion. B7 inhibited tumor growth in vivo, had no significant toxic effect on major organs and had no significant effect in vivo. In order to improve the anti-tumor effect of tetrazolium substituted pyrazine compounds, the potential side effects of B7 need further investigate in the future.

Data Sharing Statement

The data presented in this study are available in the article and Supplementary Materials.

Ethics Approval and Informed Consent

All animal studies were conducted with the approval of the Laboratory Animal Ethics Committee of Jilin University, China (approval number SY202109003). This study follows the national standard "Laboratory animal - Guideline for ethical review of animal welfare" and adopts the 3R (replacement, reduction, refinement) principles.

Acknowledgments

We are grateful to Yang Hao (Laboratory Animal Center, College of Animal Science, Jilin University, Changchun, China) for valuable discussion.

Author Contributions

All authors made a significant contribution to the work reported, whether that is in the conception, study design, execution, acquisition of data, analysis and interpretation, or in all these areas; took part in drafting, revising or critically reviewing the article; gave final approval of the version to be published; have agreed on the journal to which the article has been submitted; and agree to be accountable for all aspects of the work.

Funding

This work was funded by the Jilin Health Commission Program under Grant 2020J05S, the Fundamental Research Funds for the Central Universities under Grant 2019-JCKT-70 and 2023-JCXK-08, the Jilin Education Department Program under Grant JJKH20200950KJ, the Jilin Scientific and Technological Development Program under Grant 20190103071JH, 202002006JC, 20210101010JC and 20220505033ZP, and the Jilin Development and Reform Commission under Grant 2023C028-6.

Disclosure

The authors report no conflicts of interest in this work.

References

1. Brenner H, Hoffmeister M. [Colorectal cancer screening: evidence and implementation]. Darmkrebsfruherkennung: evidenz und Umsetzung. *Bundesgesundheitsblatt Gesundheitsforschung Gesundheitsschutz*. 2014;57(3):302–306. German. doi:10.1007/s00103-013-1911-2
2. Cunningham D, Atkin W, Lenz HJ, et al. Colorectal cancer. *Lancet*. 2010;375(9719):1030–1047. doi:10.1016/S0140-6736(10)60353-4
3. Keum N, Giovannucci E. Global burden of colorectal cancer: emerging trends, risk factors and prevention strategies. *Nat Rev Gastroenterol Hepatol*. 2019;16(12):713–732. doi:10.1038/s41575-019-0189-8
4. Veldkamp R, Gholghesaei M, Bonjer HJ, et al. Laparoscopic resection of colon Cancer: consensus of the European Association of Endoscopic Surgery (EAES). *Surg Endosc*. 2004;18(8):1163–1185. doi:10.1007/s00464-003-8253-3
5. Biagi JJ, Raphael MJ, Mackillop WJ, Kong W, King WD, Booth CM. Association between time to initiation of adjuvant chemotherapy and survival in colorectal cancer: a systematic review and meta-analysis. *JAMA*. 2011;305(22):2335–2342. doi:10.1001/jama.2011.749
6. Goldberg RM, Sargent DJ, Morton RF, et al. A randomized controlled trial of fluorouracil plus leucovorin, irinotecan, and oxaliplatin combinations in patients with previously untreated metastatic colorectal cancer. *J Clin Oncol*. 2004;22(1):23–30. doi:10.1200/JCO.2004.09.046
7. Blondy S, David V, Verdier M, Mathonnet M, Perraud A, Christou N. 5-Fluorouracil resistance mechanisms in colorectal cancer: from classical pathways to promising processes. *Cancer Sci*. 2020;111(9):3142–3154. doi:10.1111/cas.14532

8. Lee S, LaCour TG, Fuchs PL. Chemistry of trisdecacyclic pyrazine antineoplastics: the cephalostatins and ritterazines † This review is dedicated to the community of isolation/identification natural product detectives, with special thanks to the groups of Bob Pettit and Nobuhiro Fusatani. *Chem Rev*. 2009;109(6):2275–2314. doi:10.1021/cr800365m
9. Juhás M, Zitko J. Molecular Interactions of Pyrazine-Based Compounds to Proteins. *J Med Chem*. 2020;63(17):8901–8916. doi:10.1021/acs.jmedchem.9b02021
10. Dolezal M, Zitko J. Pyrazine derivatives: a patent review (June 2012 – present). *Expert Opin Ther Pat*. 2015;25(1):33–47. doi:10.1517/13543776.2014.982533
11. Miniyar BP, Murumkar RP, Patil SP, Barmade AM, Bothara GK. Unequivocal role of pyrazine ring in medicinally important compounds: a review. *Mini Rev Med Chem*. 2013;13(11):1607–1625. doi:10.2174/1389557511313110007
12. Dubuisson MLN, Rees JF, Marchand-Brynaert J. Discovery and validation of a new family of antioxidants: the aminopyrazine derivatives. *Mini Rev Med Chem*. 2004;4(4):421–435. doi:10.2174/1389557043403927
13. Huigens RW, Brummel BR, Tenneti S, Garrison AT, Xiao T. Pyrazine and phenazine heterocycles: platforms for total synthesis and drug discovery. *Molecules*. 2022;27(3):1112. doi:10.3390/molecules27031112
14. Dhiman N, Kaur K, Jaitak V. Tetrazoles as anticancer agents: a review on synthetic strategies, mechanism of action and SAR studies. *Bioorg Med Chem*. 2020;28(15):115599. doi:10.1016/j.bmc.2020.115599
15. Gao F, Xiao J, Huang G. Current scenario of tetrazole hybrids for antibacterial activity. *Eur J Med Chem*. 2019;184:111744. doi:10.1016/j.ejmech.2019.111744
16. Zhang J, Wang S, Ba Y, Xu Z. Tetrazole hybrids with potential anticancer activity. *Eur J Med Chem*. 2019;178:341–351. doi:10.1016/j.ejmech.2019.05.071
17. Gao C, Chang L, Xu Z, et al. Recent advances of tetrazole derivatives as potential anti-tubercular and anti-malarial agents. *Eur J Med Chem*. 2019;163:404–412. doi:10.1016/j.ejmech.2018.12.001
18. Myznikov LV, Vorona SV, Zevatskii YE. Biologically active compounds and drugs in the tetrazole series. *Chem Heteroc Comp*. 2021;57(3):224–233. doi:10.1007/s10593-021-02897-4
19. Neochoritis CG, Zhao T, Dömling A. Tetrazoles via multicomponent reactions. *Chem Rev*. 2019;119(3):1970–2042. doi:10.1021/acs.chemrev.8b00564
20. Herr RJ. 5-Substituted-1H-tetrazoles as carboxylic acid isosteres: medicinal chemistry and synthetic methods. *Bioorg Med Chem*. 2002;10(11):3379–3393. doi:10.1016/S0968-0896(02)00239-0
21. Wächter GA, Davis MC, Martin AR, Franzblau SG. Antimycobacterial activity of substituted isosteres of pyridine- and pyrazinecarboxylic acids. *J Med Chem*. 1998;41(13):2436–2438. doi:10.1021/jm9708745
22. Tisseh ZN, Dabiri M, Nobahar M, Soorki AA, Bazgir A. Catalyst-free synthesis of N-rich heterocycles via multi-component reactions. *Tetrahedron*. 2012;68(16):3351–3356. doi:10.1016/j.tet.2012.02.051
23. Bornscheuer UT, Huisman GW, Kazlauskas RJ, Lutz S, Moore JC, Robins K. Engineering the third wave of biocatalysis. *Nature*. 2012;485(7397):185–194. doi:10.1038/nature11117
24. Hanefeld U, Hollmann F, Paul CE. Biocatalysis making waves in organic chemistry. 10.1039/D1CS00100K. *Chem Soc Rev*. 2022;51(2):594–627. doi:10.1039/D1CS00100K
25. Li F, Tang X, Xu Y, et al. A dual-protein cascade reaction for the regioselective synthesis of quinoxalines. *Org Lett*. 2020;22(10):3900–3904. doi:10.1021/acs.orglett.0c01186
26. Li F, Su J, Xu Y, et al. A glucose oxidase-hemoglobin system for efficient oxysulfonylation of alkenes/alkynes in water. *Molecul Cata*. 2021;500:111336. doi:10.1016/j.mcat.2020.111336
27. Yang Y, Arnold FH. Navigating the unnatural reaction space: directed evolution of heme proteins for selective carbene and nitrene transfer. *Acc Chem Res*. 2021;54(5):1209–1225. doi:10.1021/acs.accounts.0c00591
28. Levine B, Mizushima N, Virgin HW. Autophagy in immunity and inflammation. *Nature*. 2011;469(7330):323–335. doi:10.1038/nature09782
29. White E. Deconvoluting the context-dependent role for autophagy in cancer. *Nat Rev Cancer*. 2012;12(6):401–410. doi:10.1038/nrc3262
30. Zhao RY, Fu JH, Zhu LJ, Chen Y, Liu B. Designing strategies of small-molecule compounds for modulating non-coding RNAs in cancer therapy. *J Hematol Oncol*. 2022;15(1). doi:10.1186/s13045-022-01230-6
31. Ismail NI, Othman I, Abas F, Naidu R, Naidu R. The curcumin analogue, MS13 (1,5-Bis(4-hydroxy-3- methoxyphenyl)-1,4-pentadiene-3-one), inhibits cell proliferation and induces apoptosis in primary and metastatic human colon cancer cells. *Molecules*. 2020;25(17):3798. doi:10.3390/molecules25173798
32. Brockmueller A, Buhrmann C, Shayan P, Shakibaei M. Resveratrol induces apoptosis by modulating the reciprocal crosstalk between p53 and Sirt-1 in the CRC tumor microenvironment. *Front Immunol*. 2023;14:1225530. doi:10.3389/fimmu.2023.1225530
33. Flanagan L, Meyer M, Fay J, et al. Low levels of Caspase-3 predict favourable response to 5FU-based chemotherapy in advanced colorectal cancer: caspase-3 inhibition as a therapeutic approach. *Cell Death Dis*. 2016;7(2):e2087. doi:10.1038/cddis.2016.7
34. Sun C, Liu H, Guo J, et al. MicroRNA-98 negatively regulates myocardial infarction-induced apoptosis by down-regulating Fas and caspase-3. *Sci Rep*. 2017;7(1):7460. doi:10.1038/s41598-017-07578-x
35. Zhang Y, Fang J, Ma H. Inhibition of miR-182-5p protects cardiomyocytes from hypoxia-induced apoptosis by targeting CIAPIN1. *Biochem Cell Biol*. 2018;96(5):646–654. doi:10.1139/bcb-2017-0224
36. Eskandari E, Eaves CJ. Paradoxical roles of caspase-3 in regulating cell survival, proliferation, and tumorigenesis. *J Cell Bio*. 2022;221(6):e202201159. doi:10.1083/jcb.202201159
37. Lamkanfi M, Declercq W, Kalai M, Saelens X, Vandenabeele P. Alice in caspase land. A phylogenetic analysis of caspases from worm to man. *Cell Death Differ*. 2002;9(4):358–361. doi:10.1038/sj.cdd.4400989
38. Pop C, Salvesen GS. Human caspases: activation, specificity, and regulation. *J Biol Chem*. 2009;284(33):21777–21781. doi:10.1074/jbc.R800084200
39. Julien O, Wells JA. Caspases and their substrates. *Cell Death Differ*. 2017;24(8):1380–1389. doi:10.1038/cdd.2017.44
40. Jin P, Jiang J, Xie N, et al. MCT1 relieves osimertinib-induced CRC suppression by promoting autophagy through the LKB1/AMPK signaling. *Cell Death Dis*. 2019;10(8):615. doi:10.1038/s41419-019-1844-2

41. Wei Y, An Z, Zou Z, et al. The stress-responsive kinases MAPKAPK2/MAPKAPK3 activate starvation-induced autophagy through Beclin 1 phosphorylation. *Elife*. 2015;4. doi:10.7554/eLife.05289
42. Izadi M, Ali TA, Pourkarimi E. Over fifty years of life, death, and cannibalism: a historical recollection of apoptosis and autophagy. *Int J Mol Sci*. 2021;22(22):12466. doi:10.3390/ijms222212466
43. Song S, Tan J, Miao Y, Li M, Zhang Q. Crosstalk of autophagy and apoptosis: involvement of the dual role of autophagy under ER stress. *J Cell Physiol*. 2017;232(11):2977–2984. doi:10.1002/jcp.25785
44. Su W, Liao M, Tan H, et al. Identification of autophagic target RAB13 with small-molecule inhibitor in low-grade glioma via integrated multi-omics approaches coupled with virtual screening of traditional Chinese medicine databases. *Cell Prolif*. 2021;54(12):e13135. doi:10.1111/cpr.13135
45. Tian SS, Chen Y, Yang B, et al. F1012-2 inhibits the growth of triple negative breast cancer through induction of cell cycle arrest, apoptosis, and autophagy. *Phytother Res*. 2018;32(5):908–922. doi:10.1002/ptr.6030
46. Gornowicz A, Szymanowska A, Mojzych M, Czarnomysy R, Bielawski K, Bielawska A. The anticancer action of a novel 1,2,4-triazine sulfonamide derivative in colon cancer cells. *Molecules*. 2021;26(7):2045. doi:10.3390/molecules26072045
47. Huang Q, Zhan L, Cao H, et al. Increased mitochondrial fission promotes autophagy and hepatocellular carcinoma cell survival through the ROS-modulated coordinated regulation of the NFKB and TP53 pathways. *Autophagy*. 2016;12(6):999–1014. doi:10.1080/15548627.2016.1166318
48. Liang XH, Kleeman LK, Jiang HH, et al. Protection against fatal Sindbis virus encephalitis by beclin, a novel Bcl-2-interacting protein. *J Virol*. 1998;72(11):8586–8596. doi:10.1128/JVI.72.11.8586-8596.1998
49. Park JM, Huang S, Wu TT, Foster NR, Sinicrope FA. Prognostic impact of Beclin 1, p62/sequestosome 1 and LC3 protein expression in colon carcinomas from patients receiving 5-fluorouracil as adjuvant chemotherapy. *Cancer Biol Ther*. 2013;14(2):100–107. doi:10.4161/cbt.22954
50. Kang KF, Wang XW, Chen XW, Tan GM, Kang ZJ. [Expression of Beclin1 in primary hepatocellular carcinoma]. *Nan Fang Yi Ke Da Xue Xue Bao*. 2009;29(1):151–153. Chinese.
51. Feng ML, Sun MJ, Xu BY, Liu MY, Zhang HJ, Wu C. Mechanism of ELL-associated factor 2 and vasohibin 1 regulating invasion, migration, and angiogenesis in colorectal cancer. *World J Gastroenterol*. 2023;29(24):3770–3792. doi:10.3748/wjg.v29.i24.3770
52. Freeman K, Saunders MP, Uthman OA, et al. Is monitoring of plasma 5-fluorouracil levels in metastatic / advanced colorectal cancer clinically effective? A systematic review. *BMC Cancer*. 2016;16:523. doi:10.1186/s12885-016-2581-x
53. Ghafouri-Fard S, Abak A, Tondro Anamag F, et al. 5-Fluorouracil: a narrative review on the role of regulatory mechanisms in driving resistance to this chemotherapeutic agent. *Front Oncol*. 2021;11:658636. doi:10.3389/fonc.2021.658636
54. Entezar-Almahdi E, Mohammadi-Samani S, Tayebi L, Farjadian F. Recent advances in designing 5-fluorouracil delivery systems: a stepping stone in the safe treatment of colorectal cancer. *Int J Nanomedicine*. 2020;15:5445–5458. doi:10.2147/ijn.S257700
55. Chauvin A, Bergeron D, Vencic J, et al. Downregulation of KRAB zinc finger proteins in 5-fluorouracil resistant colorectal cancer cells. *BMC Cancer*. 2022;22(1):363. doi:10.1186/s12885-022-09417-3
56. McQuade RM, Stojanovska V, Bornstein JC, Nurgali K. Colorectal cancer chemotherapy: the evolution of treatment and new approaches. *Curr Med Chem*. 2017;24(15):1537–1557. doi:10.2174/0929867324666170111152436